Inorganic Chemistry

ARTICLE

pubs.acs.org/IC

Lanthanide-Ion-Assisted Structural Collapse of Layered GaOOH Lattice

Boddu Sanyasi Naidu,[†] Mukesh Pandey,[‡] Jitendra Nuwad,[†] Vasanthakumaran Sudarsan,*[,†] Rajesh Kumar Vatsa,[†] Rohidas J. Kshirsagar,[‡] and C. G. Sivan Pillai[†]

[†]Chemistry Division and [‡]High Pressure and Synchrotron Radiation Physics Division, Bhabha Atomic Research Centre, Trombay, Mumbai 400085, India

Supporting Information

ABSTRACT: GaOOH nanorods were prepared by hydrolysis of $Ga(NO_3)_3 \cdot xH_2O$ by urea at ~100 °C in the presence of different amounts of lanthanide ions like Eu^{3+}, Tb^{3+}, and Dy^{3+}. On the basis of X-ray diffraction and vibrational studies, it is confirmed that layered structure of GaOOH collapses even when very small amounts of lanthanide ions (1 atom % and more) are present in the reaction medium during the synthesis of GaOOH nanorods. The incorporation of lanthanide ions at the interlayer spacing of the GaOOH lattice, followed by its reaction with OH groups that connect the layers containing edge-shared GaO_6 in GaOOH, is the reason for the collapse of the layered structure and associated amorphization. This leads to the formation of finely mixed hydroxides of lanthanide and gallium ions. These results are further confirmed by steady-state luminescence and excited-state lifetime measurements carried out on the samples. The morphology of the nanorods is maintained upon heat treatment at high temperatures like 500 and 900 °C, and during this process, the finely mixed lanthanide and gallium hydroxides facilitate diffusion of lanthanide ions into the Ga_2O_3 lattice, as revealed by the existence of strong energy transfer with an efficiency of more than 90% between the host and lanthanide ions.

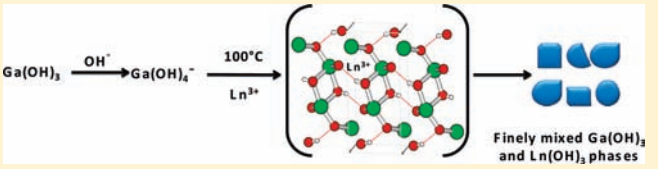

1. INTRODUCTION

Gallium oxide hydroxide is a common starting material used for the synthesis of different phases of gallium oxides, namely, α, β, γ, and ε modifications.[1,2] Different phases of Ga_2O_3 have applications such as transparent semiconducting materials for electroluminescent devices, sensor materials for absorption of molecules like CO, CO_2, alcohols, etc.[3−8] Several reports are available[9−17] on the synthesis of the GaOOH phase with different sizes and a variety of shapes. These include methods like hydrothermal treatment, sonochemical reactions, and precipitation in an aqueous medium by addition of reagents like urea, biomolecules, etc.[9−17] It is also observed that the shape is retained when the GaOOH phase is thermally decomposed to the Ga_2O_3 phase.[18,19] Doping GaOOH nanomaterials with lanthanide ions (Ln^{3+}) is an attractive option for preparing efficient luminescent materials based on lanthanide-ion-doped semiconducting Ga_2O_3 nanomaterials and thin films. A number of studies are available on the lanthanide-ion-doped Ga_2O_3 nanomaterials.[19−27] However, the effect of doping lanthanide ions on the structural aspects of GaOOH nanomaterials is not known. Because the ionic radii of Ln^{3+} and Ga^{3+} are significantly different, it is quite interesting to know where the lanthanide ions are incorporated and what structural modifications occur to the GaOOH lattice during doping. Luminescence from different lanthanide ions can be used as a probe to understand the structural changes taking place with GaOOH brought about by lanthanide ion incorporation. Such studies are essential for understanding the mechanism of lanthanide ion incorporation in different structural modifications of the Ga_2O_3 host, which are obtained by decomposition of lanthanide-ion-containing GaOOH phase. The main reason behind the lack of such studies on GaOOH:Ln^{3+} (Ln^{3+} for lanthanide ions) nanomaterials is the significant quenching of the lanthanide ion excited state brought about by vibrations of OH groups present with the GaOOH samples. For example, Li et al.[19] have carried out luminescence studies on GaOOH:Dy^{3+} nanorods and observed that Dy^{3+} emission from the sample is completely quenched. These authors also reported that thermal decomposition of GaOOH:Dy^{3+}(3%) nanorods leads to the formation of Ga_2O_3:Dy nanorods along with small amounts of the $Dy_3Ga_5O_{12}$ phase. The secondary phase might form from the Dy^{3+} ions, which are not incorporated with the GaOOH lattice. Also, considering the ionic radii of Dy^{3+} and Ga^{3+} ions under a coordination number of 6 (0.91 and 0.62 Å),[28] it is difficult to visualize that all of the Dy^{3+} ions replace Ga^{3+} in the GaOOH or Ga_2O_3 lattice.

In the present study, we investigate the effect of lanthanide ion (Eu^{3+}, Tb^{3+}, and Dy^{3+}) incorporation on the structural and morphological aspects of GaOOH nanorods. Because the luminescence properties of Eu^{3+} ions with respect to its environment are well understood, it has been used as a probe to monitor the structural changes taking place with the GaOOH lattice brought

Received: January 18, 2011
Published: April 15, 2011

about by lanthanide ion incorporation. Because the solubility product values of $Eu(OH)_3$ (9.8×10^{-27}), $Ga(OH)_3$ (7.28×10^{-36}), and GaOOH ($\sim 1 \times 10^{0.21}$)[29,30] are quite different, it is not possible for Eu^{3+} ions (lanthanide ions) to occupy the Ga^{3+} site to form phases like $Ga_{1-x}Eu_xOOH$ or $Ga_{1-x}Eu_x(OH)_3$ during the so-called coprecipitation reaction. However, when lanthanide-ion-containing GaOOH is thermally decomposed at high temperatures to form Ga_2O_3:Ln^{3+}, lanthanide ions are incorporated into the Ga_2O_3 host, as confirmed by the efficient energy transfer taking place between the host Ga_2O_3 and lanthanide ions.[19,21−23] Because the morphology of the low-temperature-synthesized GaOOH is maintained during thermal decomposition even at high temperatures (~900 °C),[19,27,31] the method has the advantage of making luminescent materials with tailor-made sizes and shapes. Hence, understanding the effect of lanthanide ion incorporation in the GaOOH lattice on its morphology and structure is important for the development of lanthanide-ion-doped Ga_2O_3 samples with different sizes and shapes. To our surprise, it has been observed in the present study that very significant changes in the structural aspects of GaOOH are taking place even with a very small amount of Eu^{3+}/Tb^{3+}/Dy^{3+} ions when present during precipitation of GaOOH. Such structural changes have been investigated through X-ray diffraction (XRD), Fourier transform infrared (FTIR), Raman, and photoluminescence techniques in the present manuscript.

2. EXPERIMENTAL SECTION

2.1. Preparation of GaOOH, α-Ga_2O_3, and β-Ga_2O_3 Nanorods. For the preparation of undoped GaOOH and lanthanide ions (Eu^{3+}, Tb^{3+}, and Dy^{3+}), doped GaOOH nanorods, $Ga(NO_3)_3 \cdot xH_2O$, $Tb(NO_3)_3 \cdot xH_2O$, $Eu(NO_3)_3 \cdot 5H_2O$, and $Dy(NO_3)_3 \cdot 5H_2O$ were used as starting materials.

In a typical procedure for making the GaOOH sample, 1 g of $Ga(NO_3)_3 \cdot xH_2O$ was dissolved in 20 mL of H_2O in a 100 mL round-bottomed flask. The solution was slowly heated up to 70 °C on a silicon oil bath with stirring, followed by the addition of 5 g of urea. The temperature was then raised to 98 °C, and the solution was refluxed until a slightly turbid solution was obtained. At this temperature, a sufficiently high concentration of OH^- is generated in the medium, leading to a high concentration of GaOOH nuclei, which facilitates growth of the nuclei into nanorod morphology. The temperature was maintained at this value for 2 h. After the reaction, the precipitate was collected by centrifugation and then washed two times with ethyl alcohol and three times with acetone, followed by drying under ambient conditions. For Eu^{3+}-, Tb^{3+}-, and Dy^{3+}-doped samples, the same procedure was used except that $Eu(NO_3)_3 \cdot 5H_2O$, $Tb(NO_3)_3 \cdot xH_2O$, and $Dy(NO_3)_3 \cdot 5H_2O$ were used, respectively, along with 1 g of $Ga(NO_3)_3 \cdot xH_2O$ and 5 g of urea as the starting materials. An aqueous solution of $Ga(NO_3)_3 \cdot xH_2O$ containing different amounts of lanthanide ions (from 0 to 2 atom % with respect to Ga^{3+} ions) was checked for its pH value before the urea addition, and the value is found to be in the range of 2.3−2.5. The pH values did not change significantly with changes in the relative concentration of the lanthanide ions in the medium. As-prepared samples were heated in a furnace to 500 and 900 °C for 10 h each to convert the GaOOH and GaOOH:Ln^{3+} phases to α and β forms of Ga_2O_3 and Ga_2O_3:Ln^{3+}.

2.2. Characterization. XRD studies were carried out using a Philips powder X-ray diffractometer (model PW 1071) with Ni-filtered Cu Kα radiation. The lattice parameters were calculated from a least-squares fitting of the diffraction peaks. The average crystallite size was calculated from the diffraction line width based on the Scherrer relation $D = 0.9\lambda/\beta \cos\theta$, where D is the average particle size, λ is the wavelength of the X-rays, and β is the full width at half-maximum.

Morphological analysis of the samples has been done using a scanning electron microscope. The instrument used was a Seron Inc. make (model AIS 2100) having a standard tungsten filament. An accelerating voltage of 20 kV and a magnification of 10K× were used for recording the micrographs. The samples were made in the form of a slurry with isopropyl alcohol and spread over a mirror-polished single crystal of a silicon substrate prior to its mounting on the stub. Energy-dispersive X-ray analysis carried out for the samples has confirmed that the relative concentrations of lanthanide ions and Ga^{3+} are in good agreement with the initial amounts taken prior to the reaction. Thermogravimetric−differential thermal analysis (TG-DTA) of the as-prepared samples was carried out in platinum crucibles using a Setaram 92-16.18 make TG-DTA instrument. In this analysis, the sample was heated under an argon environment up to 1100 °C at a heating rate of 10 °C min^{-1}. FTIR spectra were recorded for thin pellets of the samples made with KBr using a Bomem MB102 FTIR machine. Raman spectra were recorded on a homemade Raman spectrometer using 488 nm line from an air-cooled argon ion laser. The spectra were collected using a grating with 1200 grooves mm^{-1} with a slit width of ~50 μm (yielding a resolution of ~1 cm^{-1}), along with a Peltier-cooled charge-coupled device and a Razor edge filter. The raw data have a significant luminescence background, and therefore a proper background subtraction procedure has been employed. All luminescence measurements were carried out at room temperature by using an Edinburgh Instruments FLSP 920 system, having a 450 W xenon lamp and a 60 W microsecond flash lamp as excitation sources for steady-state and lifetime measurements, respectively. A red-sensitive photomultiplier tube was used as the detector. Around 20 mg of sample was mixed with 2 drops of methanol, which was made into a slurry and spread over a glass plate and then dried under ambient conditions prior to luminescence measurements. All emission spectra were corrected for the detector response and all excitation spectra for the lamp profile. All emission measurements were carried out with a resolution of 5 nm.

3. RESULTS AND DISCUSSION

Parts a−e of Figure 1 show the XRD patterns of as-prepared samples containing different amounts of Eu^{3+} ions. The as-prepared

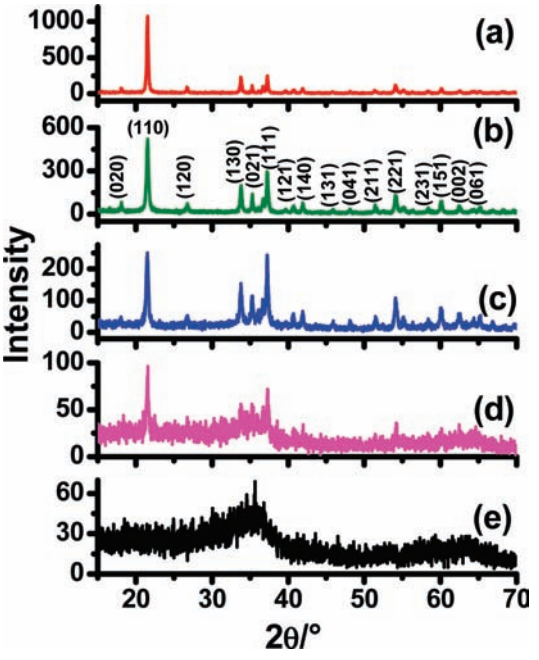

Figure 1. XRD patterns of GaOOH samples prepared in the presence of (a) 0, (b) 0.5, (c) 0.75, (d) 1, and (e) 2 atom % of Eu^{3+} ions.

dx.doi.org/10.1021/ic200106j |Inorg. Chem. 2011, 50, 4463–4472

GaOOH sample without any Eu^{3+} ions is highly crystalline with an orthorhombic crystal structure (JCPDS no. 06-0180). With an increase in the Eu^{3+} concentration, there is a slight increase in the line widths of the different diffraction peaks, and for samples prepared in the presence of more than 1 atom % Eu^{3+}, no sharp peak characteristic of the crystalline materials is observed; instead, a broad peak characteristic of the amorphous nature appeared. The lattice parameters have been calculated for the crystalline samples based on a least-squares fitting of the diffraction peaks and are found to be the same within experimental errors for all of the samples prepared in the presence of different amounts of Eu^{3+} ions, as can be seen from Table 1. On the basis of these results, it is inferred that the Eu^{3+} ions do not replace Ga^{3+} ions in the lattice of GaOOH. It is also in accordance with the significantly different ionic radii of the Ga^{3+} and Eu^{3+} ions (0.62 and 0.947 Å, respectively),[28] under a coordination number of 6. However, broadening of the peaks and conversion of crystalline GaOOH to an amorphous phase with an increase in the Eu^{3+} concentration suggests that the GaOOH lattice is affected by the presence of Eu^{3+} in the reaction medium. Similar results are also observed with Dy^{3+}- and Tb^{3+}-doped samples, and their corresponding XRD patterns are shown in Figure S-1 of the Supporting Information. The fact that even the presence of around 2 atom % $Eu^{3+}/Tb^{3+}/Dy^{3+}$ during the precipitation process of GaOOH can significantly affect its crystallinity prompted us to investigate the role played by lanthanide ions in the structural changes and associated stability of GaOOH nanorods. Hence, detailed structural and morphological investigations have been carried out on the samples and are described below.

Table 1. Variation in the Lattice Parameters of GaOOH Samples Prepared in the Presence of Different Amounts of Eu^{3+} Ions

	GaOOH			
atom % Eu^{3+}	*a* (Å)	*b* (Å)	*c* (Å)	cell volume (Å^3)
0	4.546(2)	9.797(2)	2.972(3)	132.35(2)
0.5	4.544(3)	9.786(2)	2.976(3)	132.32(2)
0.75	4.541(3)	9.787(3)	2.975(2)	132.23(3)
1	4.527(4)	9.805(3)	2.975(2)	132.05(4)

Figure 2 shows scanning electron microscopy (SEM) images of GaOOH samples prepared in the presence of different amounts of Eu^{3+} ions. The GaOOH sample prepared in the absence of Eu^{3+} ions showed rodlike morphology, as can be seen from Figure 2a. The rods have lengths of around 2.5−3 μm and widths of around 300−400 nm. Similar rodlike morphology has also been observed by number of authors for GaOOH samples prepared by urea addition as well as by hydrothermal methods.[19,27,31] For the GaOOH sample prepared in the presence of 0.5 atom % Eu^{3+} ions, the nanorods have lengths of around 1.5−2 μm and widths of around 200−300 nm (Figure 2b). However, when the GaOOH sample is prepared in the presence of 1.0 atom % Eu^{3+} ions, along with nanorods, a significantly aggregated/agglomerated phase (with irregular shape) is also formed, as can be seen from the SEM image shown in Figure 2c. The nanorods have sizes in the range of 0.5−2 μm and widths of

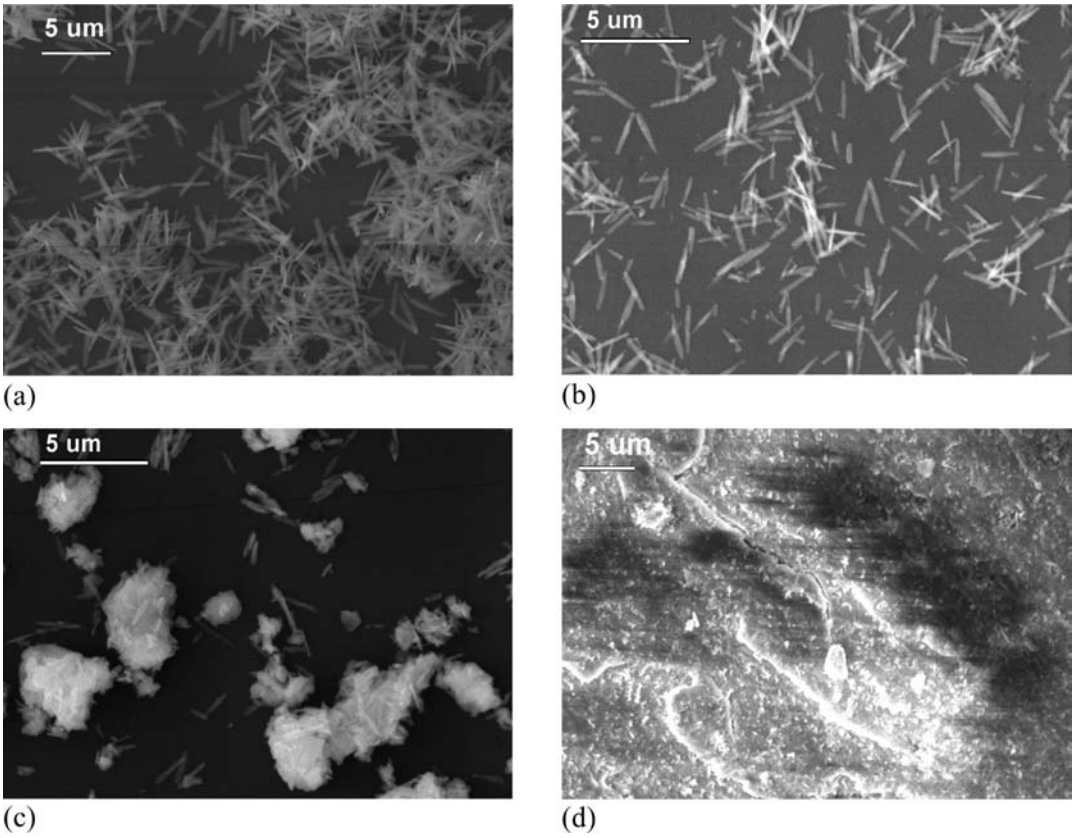

Figure 2. SEM images of GaOOH nanorods prepared in the presence of (a) 0 atom % Eu^{3+}, (b) 0.5 atom % Eu^{3+}, (c) 1 atom % Eu^{3+}, and (d) 2 atom % Eu^{3+}.

dx.doi.org/10.1021/ic200106j |*Inorg. Chem.* 2011, 50, 4463–4472

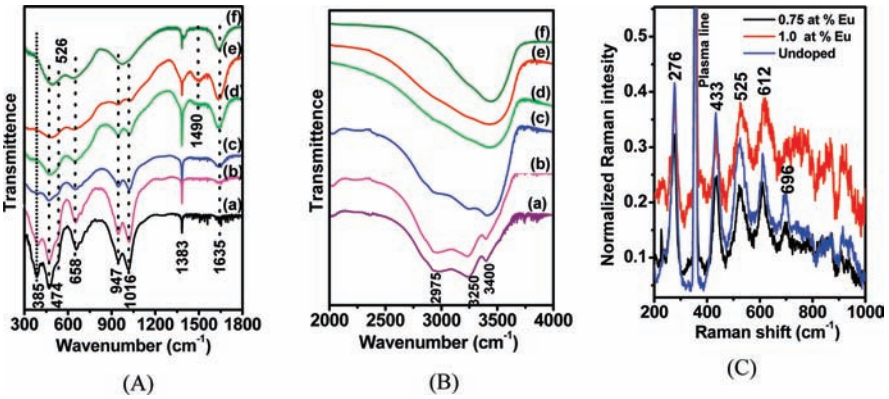

Figure 3. FTIR patterns (A and B) of GaOOH samples prepared in the presence of (a) 0, (b) 0.5, (c) 0.75, (d) 1, and (e) 2 atom % of Eu^{3+} ions and (f) amorphous $Ga(OH)_3$. The Raman spectra from the representative samples are shown in part C.

around 200 nm. No nanorod formation is observed for samples containing more than 1 atom % Eu^{3+} ions; instead, an aggregated bulk phase is observed in the representative SEM image, as can be seen from Figure 2d. On the basis of the XRD and SEM results, it is inferred that the presence of Eu^{3+} ions prevents the formation of GaOOH nanorods or destroys the layered structure of GaOOH. In order to thoroughly understand the role of Eu^{3+} ions in the formation of the GaOOH phase or in the structural changes of the GaOOH lattice, it is necessary to know the structural features of GaOOH and linkages between the basic building units constituting the GaOOH lattice.

The GaOOH phase has a structure similar to that of the mineral diaspore [α-AlO(OH)].[32] Hence, in the GaOOH structure, each gallium atom is surrounded by six oxygen atoms, forming an irregular octahedron. Each octahedron shares edges with four neighboring GaO_6 octahedra to form double chains along the *c* axis. This structure consists of two nonequivalent axial oxygen atoms, namely, O_a and O_b. One of the octahedral axes, i.e., GaO_a, is almost normal to the equatorial plane with gallium at the center, while the other octahedral axis formed with GaO_b is slightly tilted from the normal. These nonequivalent oxygen atoms (O_a and O_b) form two different kinds of OH linkages in the GaOOH structure, with one of the axial oxygen atom (O_b) bonded directly to hydrogen, while another oxygen atom (O_a) is bonded with hydrogen of the neighboring octahedron. Detailed vibrational studies were carried out using infrared (IR) and Raman spectroscopic techniques for understanding the effect of Eu^{3+} incorporation on the structure of the GaOOH lattice. IR patterns corresponding to GaOOH samples prepared in the presence of different amounts of Eu^{3+} ions are shown in Figure 3A,B. For the purpose of a direct comparison, the IR pattern of $Ga(OH)_3$ prepared by the addition of ammonium hydroxide to a Ga^{3+} solution is also shown in the same figure [Figure 3A(f)]. GaOOH nanorods prepared without any Eu^{3+} ions are characterized by sharp peaks at 1016, 947, 658, 526, 474, and 385 cm^{-1} (Figure 3A) along with a broad peak in the region of 3670−2640 cm^{-1} (Figure 3B). Let us first consider the affect of Eu^{3+} addition, as seen in Figure 3A. The peaks at 385 and 526 cm^{-1} disappear with Eu^{3+} incorporation, while the peaks at ∼474, 658, 947, and 1016 cm^{-1} broaden. Also, new modes start to appear at 1490 and 1635 cm^{-1}, which are absent in the pure GaOOH sample. Similar changes are also observed in the Raman spectra (Figure 3C). The signal-to-noise ratio of the Raman spectrum degraded significantly when the Eu^{3+} content increased beyond 1 atom %. The Raman spectrum of samples without Eu^{3+} incorporation shows well-pronounced peaks at ∼276, 433, 526, 612, and 696 cm^{-1}. With Eu^{3+} incorporation, the widths of the Raman peaks at ∼526 and 612 cm^{-1} increase because of the development of additional shoulder peaks at ∼550 and ∼650 cm^{-1} and are attributed to GaOOH lattice distortions. A summary of the peaks observed with different samples with possible assignments, together with that observed in $Ga(OH)_3$, is given in Table 2. Because the peaks are significantly overlapping, deconvolution of the individual peaks from the IR patterns could not be performed for estimation of the line width. Even though there is a broadening of the peaks with an increase in the Eu^{3+} content, the peak positions corresponding to different vibrational modes in these samples remain the same within experimental error.

The regular GaO_6 octahedron has an O_h symmetry and, in principle, should have 15 modes having symmetry $\Gamma_{vib} = A_{1g}(R) + E_g(R) + 2T_{1g}(IR) + T_{2g}(R) + T_{2u}$.[33] The prominent Raman modes in such a regular octahedron are observed at 526 cm^{-1} (A_{1g}), 430 cm^{-1} (E_g), and 328 cm^{-1} (T_{2g}). The only mode observed in IR is found at around 510 cm^{-1}. However, in GaOOH, the GaO_6 octahedron is distorted and, hence, many more modes become active in IR. According to Zhao et al.,[34] the peaks at 276, 433, and 526 cm^{-1} are due to the associated GaOH units of the α-GaO(OH) phase. The 474 cm^{-1} peak in IR has been assigned to the stretching mode of GaO_2 chains. The peak at 385 cm^{-1} is attributed to the deformation mode corresponding to GaO_6 and was reported by different groups,[35−37] in both GaOOH and β-Ga_2O_3. This is because both GaOOH and Ga_2O_3 are made up of GaO_6 octahedra as basic building units. Peaks at around 1016 and 947 cm^{-1} arise because of the δ(OH) deformation vibrations.[9] The peaks at ∼612 and 696 cm^{-1} observed in Raman spectra are, however, not clearly understood, but these peaks were also observed in the GaOOH nanorods prepared by Zhao et al.[34] The disappearance of peaks at 385 and 526 cm^{-1}, together with the reduced intensity of other peaks, clearly indicates that Eu^{3+} incorporation results in disruption of the basic building blocks of the GaOOH phase. When the latter is compared with an amorphous $Ga(OH)_3$ sample, we observe that similar features are present in the $Ga(OH)_3$ sample also, indicating that the crystal structure is disrupted with the Eu^{3+} addition, and finally with more than 1 atom % Eu^{3+}, it is fully disrupted. This is further evident by newly appearing peaks at ∼1490 and 1635 cm^{-1} for GaOOH samples having higher Eu^{3+}

dx.doi.org/10.1021/ic200106j |*Inorg. Chem.* 2011, 50, 4463–4472

Table 2. Summary of Important Modes of Vibrations in GaOOH Nanorods Containing Different Amounts of Eu^{3+} Ions along with That of $Ga(OH)_3$

frequencies in GaOOH (0% Eu)	GaOOH/0.75% Eu	GaOOH/1% Eu	$Ga(OH)_3$	assignment
3400 (IR)	3410	3430	3440	OH stretching (physisorbed H_2O)
3250 (IR)	3254 (w, br)[a]			OH stretching (non-hydrogen-bonded)
2975 (IR)	2940 (w, br)[a]			OH stretching (hydrogen-bonded)
1635 (IR)	1638	1641	1634	OH bending modes
1016 (IR)	1016	1014	973 (br)	δ(OH) deformation modes
947 (IR)	944	941		
658 (IR)	646	640	633	Ga−O vibrations
612 (R)	611	608		lattice modes
526 (R)	525	522		stretching modes of GaO_6 octahedra
474 (IR)	464	470	490	stretching vibrations of GaO_2 chains
433 (R)	430	425		
385 (IR)	387			deformation mode of a GaO_6 octahedron
276 (R)	274			

[a] w, br means a weak and broad peak.

concentrations (Figure 3A). On the basis of the previous IR studies of rare-earth hydroxides like $La(OH)_3$[38] and the pattern corresponding to $Ga(OH)_3$ shown in Figure 3A(f), the peaks at 1490 and 1635 cm^{-1} have been attributed to the bending vibrations of the OH groups associated with $Eu(OH)_3$ and $Ga(OH)_3$ phases, respectively. Another peak at 1383 cm^{-1}, which is present in the FTIR patterns of all of the samples, arises because of adsorbed carbonate species[19,39] formed during sample preparation. The structure of GaOOH affected by Eu^{3+} incorporation is also seen in the high-frequency region at ∼3500−2600 cm^{-1}. This may be considered as the overlapping of peaks at around 3400, 3250, and 2975 cm^{-1} (Figure 3B). From the previous vibrational studies[19,30,31,40−43] on GaOOH and AlOOH (which have structures similar to that of GaOOH), the peak at around 3400 cm^{-1} can be attributed to the OH stretching vibrations of physisorbed H_2O molecules, while those at 2975 and 3250 cm^{-1} may be attributed to the two different kinds of OH bonds associated with its structure. As explained previously, in the basic building unit of GaOOH, the two nonequivalent oxygen atoms in the GaO_6 octahedron are bound differently to the adjacent hydrogen atoms. One of the oxygen atoms is bound directly to hydrogen, while the other one is bound via hydrogen bonding, causing differences in their bond strengths. The peak at ∼2975 cm^{-1} is attributed to the stretching vibrations of the OH groups, which are hydrogen-bonded to GaO_6 octahedra, while the peak at ∼3250 cm^{-1} is due to non-hydrogen-bonded OH linkages. The systematic disappearance of these two frequencies in the Eu^{3+}-containing GaOOH sample indicates that Eu^{3+}, in fact, affects the lattice structure through OH linkages. In the text below, we try to understand the structural changes taking place in the GaOOH lattice with Eu^{3+} incorporation.

At this stage, it is necessary to understand how the GaOOH phase is formed and how different types of linkages in the GaOOH lattice are affected by interactions with lanthanide ions. Under alkaline conditions, GaOOH is thought to form from $Ga(OH)_4^-$ species formed in the solution by the following reaction.[11] $Ga(OH)_4^-$ upon thermal decomposition at ∼100 °C leads to the GaOOH phase.

$$Ga^{3+} \xrightarrow{OH^-} Ga(OH)_3 \xrightarrow{OH^-} Ga(OH)_4^-(aq) \xrightarrow{\sim 100\ ^\circ C} GaOOH(s) + OH^-(aq) + H_2O$$

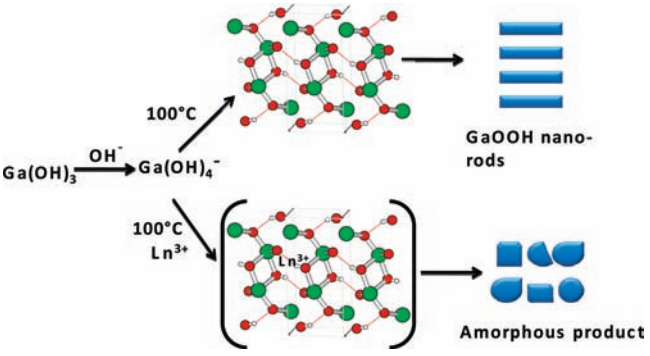

Figure 4. GaOOH structure obtained using the software *Moldraw*, depicting interaction of the Eu^{3+} ions with the GaOOH lattice and collapse of its layered structure to form amorphous gallium and europium hydroxide. Color code: green spheres represent gallium, red spheres represent oxygen, and white spheres represent hydrogen. Dotted red lines represent hydrogen bonding.

A schematic representation of a fragment of the GaOOH lattice, depicting GaO_6 octahedra, O tetrahedra, and hydrogen atoms attached with oxygen atoms, obtained by the simulation program *Moldraw*,[44] is shown in Figure 4. The unit cell is shown within the rectangle drawn with a light-black line. Hydrogen bonds existing between the layers stabilize the layered structure of GaOOH. When lanthanide ions like Eu^{3+} is present in the reaction medium, because of the higher solubility product of lanthanide hydroxides [$Ln(OH)_3$] compared to $Ga(OH)_3$,[29] $Ga(OH)_3$ is formed initially, and the latter reacts with OH^- in the reaction medium to form $Ga(OH)_4^-$. Because the concentrations of Eu^{3+} ions are much smaller than those of Ga^{3+}, it is quite possible that each Eu^{3+} ion will have a number of $Ga(OH)_4^-$ species in their vicinity. For the purpose of a charge-neutrality minimum of three anionic species, $Ga(OH)_4^-$ must surround the Eu^{3+} ions. Upon decomposition of Eu^{3+}:3$Ga(OH)_4^-$ species to GaOOH:Eu at ∼100 °C, Eu^{3+} ions can either migrate to the Ga^{3+} site in the GaOOH lattice or occupy the space between the layers of GaOOH. Because of the smaller ionic radius of Eu^{3+} compared to the interlayer spacing of GaOOH (∼2.5 Å),[45] Eu^{3+} ions/species have a tendency to be incorporated at the interlayers of GaOOH, wherein it can preferentially

dx.doi.org/10.1021/ic200106j |*Inorg. Chem.* 2011, 50, 4463–4472

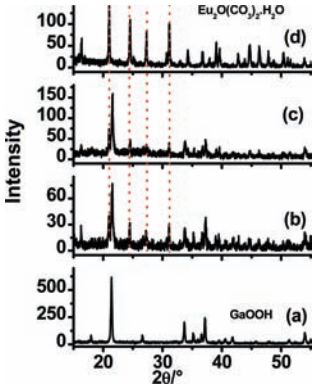

Figure 5. XRD patterns corresponding to GaOOH nanorods treated with an aqueous solution of Eu^{3+} ions in the presence of urea at ~100 °C for (a) 0, (b) 30, and (c) 2 h. The corresponding pattern obtained only with Eu^{3+} ions in the absence of GaOOH is shown in part d.

interact with OH groups to form europium hydroxide species. The formation of such hydroxide species destabilizes the layered structure of GaOOH. Because each Eu^{3+} ion can react with three OH groups, small amounts of Eu^{3+} in GaOOH are sufficient to create significant destabilization of the lattice, leading to collapse of its structure and associated amorphization. These changes are schematically shown in Figure 4. There is another possibility that the protons of the OH linkages can undergo ion exchange with the Eu^{3+} ions, and this, in turn, can lead to collapse of the layered GaOOH structure. In order to check this aspect, ion-exchange studies were carried out and are described below.

Figure 5 shows the XRD patterns of the product obtained by mixing GaOOH nanorods with an aqueous solution of europium nitrate heated in the presence of urea for 30 min and 2 h around 100 °C (samples were isolated after treatment by centrifugation). The XRD pattern of the obtained product after 30 min and 2 h of heat treatment is found to be mainly GaOOH, as can be seen from Figure 5b,c. With an increase in the time duration, a crystalline phase of Eu^{3+} ions, namely, europium hydroxide carbonate, started to appear, as can be clearly seen from Figure 5c. For the purpose of comparison, Eu^{3+} ions alone in water are subjected to urea treatment, as described above for 2 h of treatment, and the XRD pattern of the precipitate is shown in Figure 5d. The pattern matches well with that of the crystalline europium hydroxide carbonate phase (PC-PDF no. 43-0603). These results further confirm that the ion-exchange process is not responsible for collapse of the layered structure of GaOOH; instead, Eu^{3+} incorporation at the interlayer spacing and its reaction with OH groups at the interlayer spacing are the reasons for amorphization. Such an amorphization process is also expected to have a significant effect on the luminescence properties of lanthanide ions and, hence, detailed luminescence studies were carried out for these samples and are described below.

Figure 6 shows the emission and excitation spectra of as-prepared GaOOH nanorods prepared in the absence of any lanthanide ions (Eu^{3+}). The emission spectrum matches with that reported by Huang and Yeh.[31] The emission spectrum is characterized by a peak at around 435 nm, which arises from the electronic transition involving Ga−O bonds in the GaO_6 octahedra. On the basis of the photoluminescence studies of a variety of gallium compounds containing GaO_6 octahedra,[31,46−49] the emission at around 435 nm has been attributed to the recombination of electrons trapped at oxygen vacancies and hole trapped

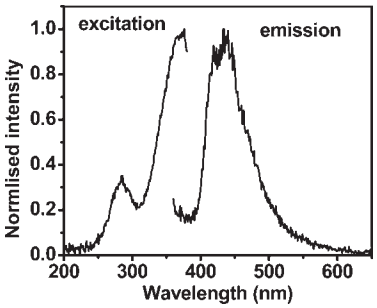

Figure 6. Emission spectrum obtained after 280 nm excitation and excitation spectrum corresponding to a 435 nm emission from GaOOH nanorods prepared in the absence of any Eu^{3+} ions.

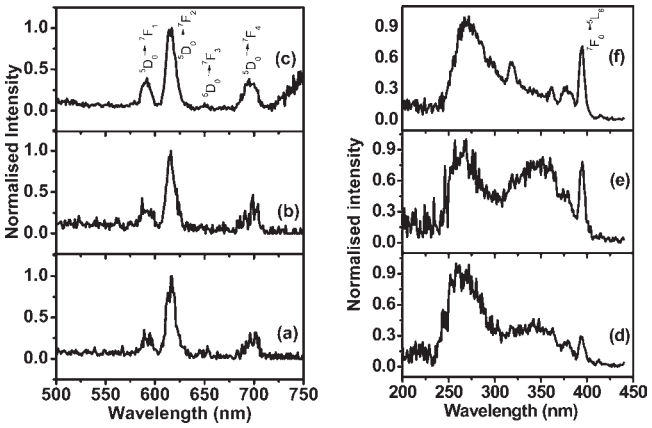

Figure 7. Emission spectrum (left) obtained at 350 nm and excitation and excitation spectra (right) corresponding to a 615 nm emission from GaOOH nanorods prepared in the presence of (a and d) 0.5 atom % Eu^{3+}, (b and e) 0.75 atom % Eu^{3+}, and (c and f) 2 atom % Eu^{3+}.

at Ga^{3+} vacancies present in GaOOH. The corresponding excitation spectrum is characterized by peaks at around 360 and 280 nm. UV−visible optical absorption studies[31] have revealed that GaOOH has an optical band gap at around 4.4 eV (~280 nm), and hence the excitation peak at around 280 nm is assigned to excitation of the electron from the valence band to the conduction band of the GaOOH phase. The other excitation peak at around 360 nm is attributed to excitation of electrons from the valence band to defect levels (oxygen vacancies) present in the lattice. The existence of energy transfer from hosts like Ga_2O_3 to lanthanide ions is used as a criterion to confirm lanthanide ion incorporation in the host. In order to find out whether the lanthanide ion is incorporated into the GaOOH lattice based on the above logic, detailed luminescence experiments were carried out for lanthanide-ion-doped GaOOH samples and are described below.

Figure 7 (right) shows the emission spectrum from GaOOH nanorods prepared in the presence of different amounts of Eu^{3+} ions. The emission spectrum is characterized by peaks mainly at around 590 and 615 nm, which are due to the magnetic- and electric-dipole-allowed $^5D_0 \rightarrow {}^7F_1$ and $^5D_0 \rightarrow {}^7F_2$ transitions, respectively, of Eu^{3+} ions. The emission spectrum is the same for all the samples, suggesting that the Eu^{3+} environment does not change with an increase in the Eu^{3+} content in the medium. The relative intensity ratio of the $^5D_0 \rightarrow {}^7F_2$ (615 nm) to $^5D_0 \rightarrow {}^7F_1$ (590 nm) transition, known as the asymmetric ratio of

dx.doi.org/10.1021/ic200106j |Inorg. Chem. 2011, 50, 4463–4472

luminescence, is found to be around 2.6 for all of the samples, further confirming that the Eu^{3+} environment is the same in all the samples. The excitation spectrum corresponding to 615 nm emission from these samples is shown in Figure 7(left). The patterns essentially consist of sharp peaks characteristic of the intra 4f transitions along with broad peak centered around 265 and 360 nm. The peak at 265 nm arises because of the Eu−O charge-transfer process, and this peak overlaps with that of the host excitation peak at around 280 nm, whereas the other peak at around 360 nm is due to excitation of electrons to the defect levels present in the GaOOH host, as can be clearly seen in the excitation spectrum corresponding to GaOOH nanorods prepared in the absence of any Eu^{3+} ions (Figure 6). The appearance of a broad host excitation peak at around 360 nm in the excitation spectrum obtained by monitoring Eu^{3+} emission at around 615 nm suggests that Eu^{3+} emission can be obtained by exciting the host at 360 nm. This is possible only when excited charge carriers in the GaOOH host transfer their energy to Eu^{3+} ions. In other words, energy transfer occurs from the host GaOOH nanorods to the Eu^{3+} species. Similar results were also observed with GaOOH:Tb and GaOOH:Dy samples. Representative emission and excitation spectra from the GaOOH:Dy sample having 1 atom % Dy^{3+} are shown in Figure S-2 of the Supporting Information. The energy-transfer efficiency (η) has been calculated from the emission spectra of GaOOH and GaOOH:Dy nanorods based on the equation $\eta = 1 - I_d/I_{d0}$, where I_d and I_{d0} are the intensities of emission in the presence and absence of Dy^{3+} ions, respectively.[19] The efficiency is found to be ~32% for the GaOOH:Dy sample. Generally, high values of the energy-transfer efficiency (on the order of 90%) are observed for lanthanide ions incorporated in hosts like Ga_2O_3. Such a low value of the energy-transfer efficiency indicates that the lanthanide ions are not incorporated in the GaOOH host and instead form a separate Ln^{3+} species, which are intimately mixed with the GaOOH/amorphous gallium hydroxide phase. Because of this intimate mixing, there can be some Ln^{3+} species close to the surface of GaOOH, and this leads to weak energy transfer.

These inferences are further substantiated by decay curves corresponding to the $^5D_0$ level of Eu^{3+} (Figure 8) from these samples. The decay has been found to be single-exponential for all of the samples with a lifetime value of around 340 μs. The values are higher than that of the europium hydroxide phase (250 μs) prepared by a method identical with that of GaOOH (the decay curve is shown in Figure S-3 of the Supporting Information). Identical lifetime values corresponding to the $^5D_4$ level of Tb^{3+} ions [1.2 ms (80%) and 388 μs (20%)] are also observed for GaOOH samples containing different amounts of Tb^{3+}, as can be seen from Figure S-4 of the Supporting Information. Hence, from the decay curves and emission spectra, it is inferred that the lanthanide hydroxide phase is finely mixed with amorphous gallium hydroxide and the crystalline GaOOH phase. These results are further supported by TG-DTA studies on the samples and are described below.

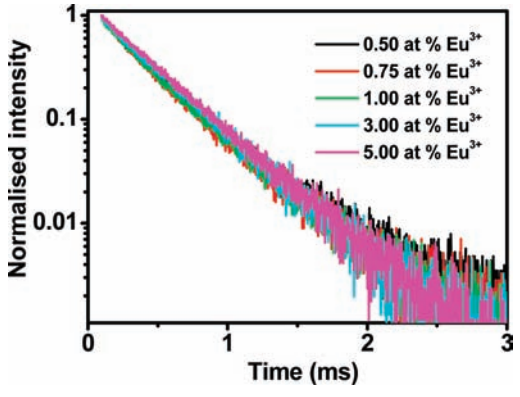

Figure 8. Decay curves corresponding to the $^5D_0$ level of Eu^{3+} ions from GaOOH samples prepared with different amounts of Eu^{3+} ions. Samples were excited at 265 nm, and emission was monitored at 615 nm.

TG-DTA patterns of the GaOOH sample prepared in the presence of different amounts of Eu^{3+} ions are shown in Figure 9. The GaOOH sample prepared in the absence of any Eu^{3+} ions is characterized by two stages of weight loss in its thermogram (Figure 9a). They are in the ranges of 200−280 and 350−420 °C and have been attributed to dehydration of the surface-bound and constitutional hydroxyl groups, respectively, present with GaOOH samples. The weight loss is around 9% in the range of 350−420 °C, confirming dehydration from the GaOOH phase.[18] Such dehydration processes are characterized by endothermic peaks at around 230 and 400 °C in the corresponding DTA pattern. Beyond 420 °C, there is no significant change in the weight with increase in temperature, as is clear from the straight line with negligible slope observed beyond 420 °C in the TG pattern shown in Figure 9a. However, the DTA pattern showed a broad exothermic peak over the region of 640−1040 °C, and this is due to conversion of the α-Ga_2O_3 phase to β-Ga_2O_3. Similar DTA peaks have also been observed by different authors[39,41] for decomposition of the GaOOH phase. For the GaOOH sample prepared in the presence of 0.5 atom % Eu^{3+} ions (Figure 9b), both of the TG and DTA patterns are essentially similar to that of GaOOH nanorods shown in Figure 9a. However, the DTA peaks are slightly broadened for the Eu^{3+}-containing sample, as can be seen from Figure 9b. Broadening of the peak has been attributed to distortion taking place with the Ga−O bonds associated with GaOH linkages brought about by their interaction with Eu^{3+} ions. The percentage loss of weight is found to be around 9% over the region of 230−400 °C, which is characteristic of the dehydration process in GaOOH. For the GaOOH sample prepared with 0.75 atom % Eu^{3+} ions (Figure 9c), the initial dehydration step over the region 200−280 °C is more predominant compared to the corresponding step for the GaOOH sample prepared with 0.5 atom % Eu^{3+}. In addition to this, the weight loss below 400 °C is found to be around 10%, suggesting that another hydroxide species along with the GaOOH phase is present with the sample. This is, namely, the $Ga(OH)_3$ phase, formed by collapse of a part of the layered GaOOH structure. However, the DTA pattern is comparable with that of the GaOOH sample prepared with 0.5 atom % Eu^{3+}. For the GaOOH sample prepared with 1 atom % Eu^{3+} ions, both of the DTA and TG patterns significantly changed, as can be seen in Figure 9d. The weight loss is also found to be around 12%, indicating an increase in the extent of the gallium hydroxide phase along with the GaOOH phase. The DTA pattern (Figure 9d) is similar to that obtained for a group 13 metal hydroxide like $In(OH)_3$[50,51] and can be considered as overlapping the DTA patterns of $Ga(OH)_3$ and GaOOH present in the sample. For the purpose of comparison, the TG and DTA patterns of $Ga(OH)_3$ in the present study are shown in Figure S-5 of the Supporting Information. From these results, it is inferred that the GaOOH phase undergoes complete decomposition in the presence of Eu^{3+} ions having concentrations more than 1 atom %, forming $Ga(OH)_3$ species. Hence,

dx.doi.org/10.1021/ic200106j |Inorg. Chem. 2011, 50, 4463–4472

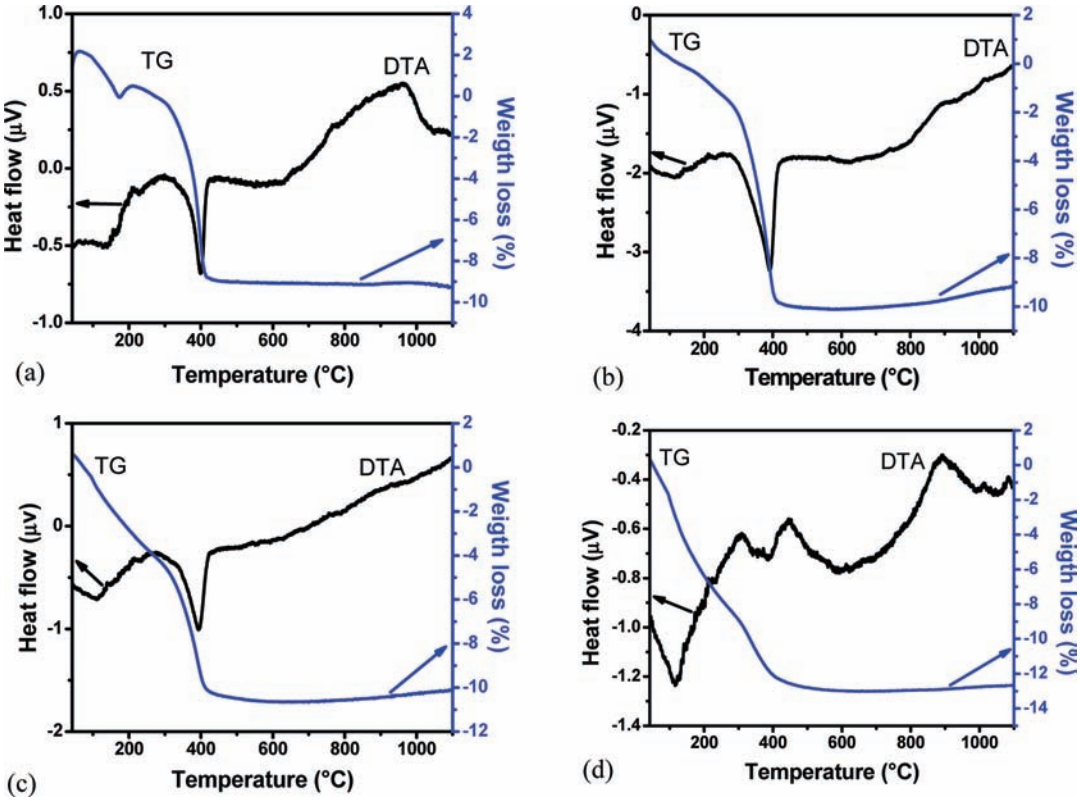

Figure 9. TG-DTA patterns of GaOOH nanorods prepared in the presence of (a) 0, (b) 0.5, (c) 0.75, and (d) 1 atom % Eu^{3+} ions.

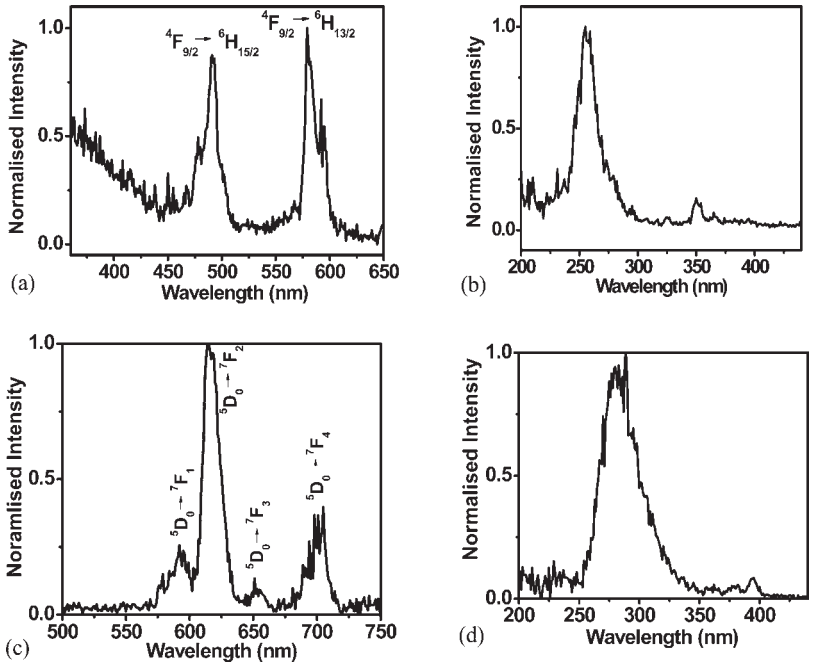

Figure 10. Emission spectrum (a) obtained after 260 nm excitation and excitation spectra (b) corresponding to a 575 nm emission from GaOOH nanorods prepared in the presence of 2 atom % Dy^{3+} ions and heated at 900 °C. Corresponding emission ($\lambda_{excitation}$ = 280 nm) and excitation ($\lambda_{emission}$ = 613 nm) spectra from Ga_2O_3/Eu nanorods are shown in Figure 10c,d.

the TG-DTA results are also in conformity with the inferences drawn from XRD and photoluminescence studies.

GaOOH and lanthanide ions containing GaOOH nanorods are converted upon heating to lanthanide-ion-doped Ga_2O_3 nanorods while maintaining their morphology, as can be seen from the XRD patterns and SEM images shown in Figures S-6 and S-7 of the Supporting Information, respectively. The emission and excitation spectra from representative Ga_2O_3:Dy and

dx.doi.org/10.1021/ic200106j |*Inorg. Chem.* 2011, 50, 4463–4472

β-Ga_2O_3:Eu samples are shown in Figure 10a−d. The emission spectrum shown in Figure 10a corresponds to β-Ga_2O_3:Dy nanorods and is obtained by exciting the host at 260 nm. The spectrum is characterized by sharp emission peaks due to intra 4f transitions of Dy^{3+} ions. The corresponding excitation spectrum obtained by monitoring the Dy^{3+} emission at 575 nm is shown in Figure 10b. Observation of host excitation at around 260 nm while monitoring the Dy^{3+} emission confirms that energy transfer occurs from host to Dy^{3+} ions in β-Ga_2O_3:Dy nanorods. A comparison of these emission and excitation spectra with that of GaOOH:Dy samples shown in Figure S-2 of the Supporting Information reveals that energy transfer is relatively stronger in the Ga_2O_3:Dy system compared to the GaOOH:Dy system. The efficiency of energy transfer has been calculated and found to be around 92% in this case. The possible reason for the improved energy transfer is the combined effect of migration of the lanthanide ions in the lattice of Ga_2O_3 and removal of the hydroxyl groups by heat treatment. These observations are in agreement with those reported on lanthanide-ion (Dy^{3+})-doped Ga_2O_3 nanomaterials.[19] Similar results are also observed from β-Ga_2O_3:Eu nanorods obtained after decomposition of GaOOH:Eu nanorods at 900 °C, as can be seen from the emission and excitation spectra shown in Figure 10c,d. The patterns match well with those reported for β-Ga_2O_3:Eu films by Mizunashi and Fujihara.[52] Unlike the excitation spectrum observed for Ga_2O_3:Dy nanorods (Figure 10b), the excitation spectrum corresponding to Ga_2O_3:Eu nanorods is characterized by a broad peak with an emission maximum at around 280 nm. This has been attributed to the overlapping of an Eu−O charge-transfer band with the Ga_2O_3 host excitation peak.

On the basis of the detailed structural and luminescence studies, it is established that very small amounts of lanthanide ion are sufficient for destruction of the layered structure of GaOOH to form an amorphous gallium hydroxide phase. The reason for collapse of the structure is due to the interaction/reaction of lanthanide ions with the hydroxyl groups existing at the interlayer spacings of GaOOH, as is evident from vibrational analysis of the OH stretching frequencies. The interaction leads to removal of the OH groups that connect different layers in the GaOOH lattice, thereby leading to its amorphization.

4. CONCLUSIONS

On the basis of XRD, SEM, and vibrational studies, it is concluded that the layered structure and morphology of GaOOH undergo significant changes even when very small amounts (~1 atom %) of lanthanide ions (for example, Eu^{3+}, Tb^{3+}, and Dy^{3+} ions) are present during its synthesis. These lanthanide ions interact with the hydroxyl groups present at the interlayers of GaOOH to form europium hydroxide, thereby disrupting the OH groups, which stabilizes the layered structure of GaOOH. This is responsible for collapse of its crystalline layered structure, leading to amorphization. Amorphous gallium and europium hydroxides, wherein the latter phase is very finely dispersed with the former, are formed during the process. TG-DTA and luminescence studies further confirm this. The existence of energy transfer between the host and dopant lanthanide ions is because of the fine dispersion of lanthanide hydroxides with gallium hydroxide and GaOOH. Upon heating, the nanorods maintain their morphology and lanthanide ions diffuse into the Ga_2O_3 lattice, as revealed by the existence of strong energy transfer between the Ga_2O_3 and lanthanide ions.

■ ASSOCIATED CONTENT

Supporting Information. XRD patterns, emission and excitation spectra, decay curves, TG-DTA patterns, and SEM images of the nanomaterials. This material is available free of charge via the Internet at http://pubs.acs.org.

■ AUTHOR INFORMATION

Corresponding Author

*E-mail: vsudar@barc.gov.in. Tel: 91-22-25590289. Fax: 91-22-25505151.

■ ACKNOWLEDGMENT

The authors thank Dr. D. Das, Head of the Chemistry Division, Dr. S. M. Sharma, Head of the High Pressure and Synchrotron Radiation Physics Division, and Dr. T. Mukherjee, Director of the Chemistry Group, BARC, for their encouragement during this work. Shri. S. Kolay of Chemistry Division, BARC, is thanked for recording the TG-DTA patterns of the samples.

■ REFERENCES

(1) Roy, R.; Hill, V. G.; Osborn, E. F. *J. Am. Chem. Soc.* **1952**, *74*, 719.
(2) Qian, H. S.; Gunawan, P.; Zhang, Y. X.; Lin, G. F.; Zheng, J. W.; Xu, R. *Cryst. Growth Des.* **2008**, *8*, 1282.
(3) Binet, L.; Gourier, D.; Minot, C. *J. Solid State Chem.* **1994**, *113*, 420.
(4) Ueda, N.; Hosono, H.; Waseda, R.; Kawazoe, H. *Appl. Phys. Lett.* **1997**, *71*, 933.
(5) Miyata, T.; Nakatani, T.; Minami, T. *Thin Solid Films* **2000**, *373*, 145.
(6) Villora, E. G.; Atou, T.; Sekiguchi, T.; Sugawara, T.; Kikuchi, M.; Fukuda, T. *Solid State Commun.* **2001**, *120*, 455.
(7) Ogita, M.; Higo, K.; Nakanishi, Y.; Hatanaka, Y. *Appl. Surf. Sci.* **2001**, *175*, 721.
(8) Shimizu, K.; Satsuma, A.; Hattori, T. *Appl. Catal., B* **1998**, *16*, 319.
(9) Yan, D.; Yin, G.; Huang, Z.; Liao, X.; Kang, Y.; Yao, Y.; Hao, B.; Gu, J.; Han, D. *Inorg. Chem.* **2009**, *48*, 6471.
(10) Sun, M.; Li, D.; Zhang, W.; Fu, X.; Shao, Y.; Li, W.; Xiao, G.; He, Y. *Nanotechnology* **2010**, *21*, 355601.
(11) Avivi, S.; Mastai, Y.; Hodes, G.; Gedanken, A. *J. Am. Chem. Soc.* **1999**, *121*, 4196.
(12) Zhao, Y.; Frost, R. L.; Martens, W. N. *J. Phys. Chem. C* **2007**, *111*, 16290.
(13) Zhang, J.; Liu, Z.; Lin, C.; Lin, J. *J. Cryst. Growth* **2005**, *280*, 99.
(14) Cha, J. N.; Shimizu, K.; Zhou, Y.; Christiansen, S. C.; Chmelka, B. F.; Stucky, G. D.; Morse, D. E. *Proc. Natl. Acad. Sci. U.S.A.* **1999**, *96*, 361.
(15) Kisailus, D.; Truong, Q.; Amemiya, Y.; Weaver, J. C.; Morse, D. E. *Proc. Natl. Acad. Sci. U.S.A.* **2006**, *103*, 5652.
(16) Kisailus, D.; Choi, J. H.; Weaver, J. C.; Yang, W.; Morse, D. E. *Adv. Mater.* **2005**, *17*, 314.
(17) Lee, I.; Kwak, J.; Haam, S.; Lee, S. Y. *J. Cryst. Growth* **2010**, *312*, 2107.
(18) Tas, A. C.; Majewski, P. J.; Aldinger, F. *J. Am. Ceram. Soc.* **2002**, *85*, 1421.
(19) Li, G.; Peng, C.; Li, C.; Yang, P.; Hou, Z.; Fan, Y.; Cheng, Z.; Lin, J. *Inorg. Chem.* **2010**, *49*, 1449.
(20) Gollakota, P.; Dhawan, A.; Wellenius, P.; Lunardi, L. M.; Muth, J. F.; Saripalli, Y. N.; Peng, H. Y; Everitt, H. O. *Appl. Phys. Lett.* **2006**, *88*, 221906.
(21) Shen, W. Y.; Pang, M. L.; Lin, J.; Fand, J. *J. Electrochem. Soc.* **2005**, *152*, H25.

(22) Fu, L.; Liu, Z.; Liu, Y.; Han, B.; Wang, J.; Hu, P.; Cao, L.; Zhu, D. *J. Phys. Chem. B* **2004**, *108*, 13074.
(23) Pang, M. L.; Shen, W. Y.; Lin, J. *J. Appl. Phys.* **2005**, *97*, 033511.
(24) Biljan, T.; Gajović, A.; Meić, Z. *J. Lumin.* **2008**, *128*, 377.
(25) Nogales, E.; Méndez, B.; Piqueras, J. *Nanotechnology* **2008**, *19*, 035713.
(26) Nogales, E.; Méndez, B.; Piqueras, J.; Garcia, J. A. *Nanotechnology* **2009**, *20*, 115201.
(27) Xie, H.; Chen, L.; Liu, Y.; Huang, K. *Solid State Commun.* **2007**, *141*, 12.
(28) Shannon, R. D. *Acta Crystallogr.* **1976**, *A32*, 751.
(29) Lide, D. R. *CRC Handbook of Chemistry and Physics*; CRC Press: Boca Raton, FL, 2008; pp 8−118.
(30) Uchida, M.; Okuwaki, A. *J. Solution Chem.* **1997**, *26*, 699.
(31) Huang, C. C.; Yeh, C. S. *New J. Chem.* **2010**, *34*, 103.
(32) Hu, Y.; Liu, X.; Xu, Z. *Miner. Eng.* **2003**, *16*, 219.
(33) Rudolph, W. W.; Pye, C. C. *Phys. Chem. Chem. Phys.* **2002**, *4*, 4319.
(34) Zhao, Y.; Frost, R. L. *J. Raman Spectrosc.* **2008**, *39*, 1494.
(35) Ristić, M.; Popvić, S.; Musić, S. *Mater. Lett.* **2005**, *59*, 1227.
(36) Rao, R.; Rao, A. M.; Xu, B.; Dong, J.; Sharma, S.; Sunkara, M. K. *J. Appl. Phys.* **2005**, *98*, 094312.
(37) Liu, X.; Qiu, G.; Zhao, Y.; Zhang, N.; Yi, R. *J. Alloys Compd.* **2007**, *439*, 275.
(38) Wang, S.; Zhao, Y.; Chen, J.; Xu, R.; Luo, L.; Zhong, S. *Superlattices Microstruct.* **2010**, *47*, 597.
(39) Liu, X.; Qiu, G.; Zhao, Y.; Zhang, N.; Yi, R. *J. Alloys Compd.* **2007**, *439*, 275.
(40) Yang, J.; Zhao, Y.; Frost, R. L. *Spectrochim. Acta* **2009**, *74*, 398.
(41) Amores, J. M. G.; Escribano, V. S.; Busca, G. *J. Mater. Chem.* **1999**, *9*, 1161.
(42) Socrates, G. *Infrared Characteristic Group Frequencies*; Wiley: New York, 1994; p 224.
(43) Demichelis, R.; Noel, Y.; Civalleri, B.; Roetti, C.; Ferrero, M.; Dovesi, R. *J. Phys. Chem. B* **2007**, *111*, 9337.
(44) Ugliengo, P. *Moldraw 2.0*, version h1; www.moldraw.unito.it.
(45) Kolesova, V. A.; Ryskin, Ya. I. *J. Struct. Chem.* **1962**, *3*, 656.
(46) Fu, L.; Liu, Y.; Hu, P.; Xiao, K.; Yu, G.; Zhu, D. *Chem. Mater.* **2003**, *15*, 4287.
(47) Kim, J. S.; Park, H. L.; Chon, C. M.; Moon, H. S; Kim, T. W. *Solid State Commun.* **2004**, *129*, 163.
(48) Harwig, T.; Kellendonk, F. *J. Solid State Chem.* **1978**, *24*, 255.
(49) Liang, C. H.; Meng, G. W.; Wang, G. Z.; Wang, Y. W.; Zhang, L. D.; Zhang, S. Y. *Appl. Phys. Lett.* **2001**, *78*, 3202.
(50) Parast, M. S. Y.; Morsali, A. *Ultrason. Sonochem.* **2011**, *18*, 375.
(51) Sato, T.; Nakumara, T. *Thermochim. Acta* **1982**, *53*, 281.
(52) Mizunashi, T.; Fujihara, S. *Electrochem. Solid-State Lett.* **2008**, *11*, J43.